Colloids and Surfaces B: Biointerfaces 182 (2019) 110390

Contents lists available at ScienceDirect

Colloids and Surfaces B: Biointerfaces

journal homepage: www.elsevier.com/locate/colsurfb

Toxicity response of highly colloidal, bioactive, monodisperse SiO_2@ $Pr(OH)_3$ hollow microspheres

Anees A. Ansari[a,*], Aslam Khan[a], Maqsood A. Siddiqui[b,c], Naushad Ahmad[d], Abdulaziz A. Al-Khedhairy[c]

[a] King Abdullah Institute for Nanotechnology, King Saud University, Riyadh 11451, Saudi Arabia
[b] Al-Jeraisy Chair for DNA Research, Zoology Department, College of Science, King Saud University, Riyadh 11451, Saudi Arabia
[c] Zoology Department, College of Science, King Saud University, Riyadh 11451, Saudi Arabia
[d] Department of Chemistry, College of Science, King Saud University, Riyadh 11451, Saudi Arabia

ARTICLE INFO

Keywords:
Optical properties
Microspheres
Lanthanides
Mesoporous
Amorphous

ABSTRACT

In a facile synthesis, highly colloidal, bioactive $Pr(OH)_3$-encapsulated silica microspheres (PSMSs) with an average diameter of 500–700 nm were successfully prepared via a sol-gel process followed by heat treatment. The phase formation, morphology, surface and optical properties of the as-synthesized PSMSs were characterized by various techniques including X-ray diffraction (XRD), thermogravimetric analysis (TGA), scanning electron microscope (SEM), transmission electron microscope (TEM), N_2-adsorption-desorption, energy dispersive X-ray (EDX) analysis, Fourier transform infrared (FTIR) and UV/vis spectroscopy. The PSMSs were semi-amorphous or ultra-small in size, highly dispersible in water, mesoporous, irregular in size and spherical in shape. The SEM images show a well-ordered broad nanoporous structure which is preserved after coating with $Pr(OH)_3$ molecules, demonstrating interaction between the optically active Pr^{3+} ion and silanol (Si − OH) groups via hydrogen bonding. Optical spectra show well-resolved weak intensity 4*f*-4*f* absorption transitions in the visible region of the Pr^{3+} ion, indicating successful grafting of the $Pr(OH)_3$ layer. Toxicity was measured by MTT and NRU assays to determine potential toxicity. Cell viability was suppressed with increasing dosage of PSMSs, but showed greater than 55% cell viability at a concentration of 200 µg/mL, resulting in low toxicity. Due to its high aqueous dispersibility, optical activity, excellent biocompatibility and low toxic nature, it could be a favorable material for biomedical and drug delivery applications.

1. Introduction

In recent years, much attention has been paid to the synthesis of silica-based micro/nanostructured materials, because they can be applied in various materials applications as well as in clinical sciences for uses that include catalysis, separation, fluorescent biolabeling/imaging, bio-detection, and drug delivery [1–9]. Due to features such as chemical inertness, eco-friendliness, easy synthesis, transparency in the visible region, high solubility, colloidal stability in aqueous media, excellent biocompatibility, and non-toxic nature they are ideal candidates for applications in various fields of biomedical sciences [2,6,7,10–28]. Reports in the literature show that silica-based micro/nanostructure materials have been used as a host or guest lattice in various optically and magnetically active multifunctional nanostructured materials [2–5,10,11,27,29–37]. Lin et al. prepared highly colloidal, spherical photonic crystals based on silica-lanthanum hydroxide [38]. Lin and his associates used mesoporous silica as a substrate for coating of some magnetic and fluorescent materials and investigated their applications in fluorescent biolabeling and drug delivery [5,27,31,33,35,39]. In this context, the combination of mesoporous silica with fluorescent lanthanides and magnetic nanostructured materials forms uniform core-shell micro/nano-composite particles. These combined nanocomposites have multifunctional properties, which have been successfully applied in applications such as fluorescent bioimaging/optical bio-probes, magnetic resonance imaging and drug delivery [5,27,34,36,37,40]. To improve these applications, there is a need to develop shape- and size-controlled nanocomposites which illustrate combined properties in a single particle [5,34,37]. Among shape-based micro/nanostructured materials, spherical micro/nanomaterials are the fastest growing field. Spherical materials have distinctive features including low effective density, high specific surface area, active surface sites, ionic intercalation, porous surfaces, high particle packaging, minimized light

* Corresponding author.
E-mail addresses: amustaqeemahmad@ksu.edu.sa, aneesaansari@gmail.com (A.A. Ansari).

https://doi.org/10.1016/j.colsurfb.2019.110390
Received 9 April 2019; Received in revised form 2 July 2019; Accepted 23 July 2019
Available online 25 July 2019

scattering on the particle surface, and excellent grafting and encapsulation ability [3,4,41,42]. Additionally, a spherical shape is an ideal & perfect morphology in photonic materials due to brighter photoluminescence, high definition, improved screen packing, narrow size distribution (0.5–2 μm), and non-aggregation in most aqueous and non-aqueous media. Up to now, in order to obtain perfect mesoporous spherical micro/nanomaterials, various synthesis processes have been developed to control the shape, size, and surface properties of designed materials including thermal decomposition, hydrothermal/solvothermal, co-precipitation, micro-emulsion, and sol-gel methods. Most of these synthetic routes suffer from major dis-advantages such as high-temperature processing, hard agglomerates, and hydrophobicity due to synthesis using high molecular weight surfactants. In contrast to these methods, the sol-gel process is a relatively easy process because of its low cost, synthesis at low temperature or room temperature, and monodisperse, non-aggregated, large scale production and high colloidal stability in most aqueous and non-aqueous solvents [3,4,41,43–45]. Additionally, due to synthesis in aqueous media, the surface of the particles is hydrophilic mainly from bridging of adjacent particles with water using hydrogen bonding or van der Waals forces and the subsequently large vessel forces produced during drying [2–5,27,30,41–43,45]. Therefore, micro/nanoparticles produced by a sol-gel method generally display excellent features such as high hydrophilicity, large specific surface area, and a higher reactivity, causing surface-anchored hydroxyl groups that favor densification compared to micro/nanoparticles produced by other aqueous or non-aqueous synthesis routes. In most literature reports, silica is applied as a shell for covering many crystalline inorganic magnetic or fluorescent core materials [2,3,5,30,36,43–46]. In those cases, silica acts as a protective insulating layer that prevents combination and controls the morphology of the final particles. However, the morphology of the as-prepared crystalline materials is often not uniform or is only weakly dispersible in aqueous media. This often results in the surface coating on the silica shell not being uniform. To avoid the disadvantages of this synthesis method, we developed a single step synthesis process for the preparation of praseodymium hydroxide grafted silica microspheres.

In the present report, we propose a simple and single-step synthesis process for optically active $Pr(OH)_3$-grafted micro-spheres as photonic materials. The surface functionalization of silica spheres through the use of phosphoric materials is an additional advantage which is especially useful in controlling inter-particle interaction and in biological research. We observed the crystalline, morphological, thermal, surface, and optical properties. The morphological character was obtained from FE-TEM and SEM images, indicating a highly monodisperse, non-agglomerated, spherical shape that is mesoporous with narrow size distribution. Surface grafting of silica spheres with lanthanide materials improves the solubility, colloidal stability, and optical properties in the solid state and in solution. Generally, crystalline materials are hydrophobic in nature and the coating of silica on the surface of these materials greatly suppresses fluorescence efficiency causing high vibration energy surface ($Si-OH$) groups through multi-photon relaxation pathways. In the proposed method we aimed to improve the photoluminescence efficiency of the materials. However, due to lack of facilities, we were unable to measure the photo luminescent properties of the materials. Surface and optical properties were measured and it was found that surface hydroxyl groups and 4f-electrons make $Pr(OH)_3$ highly useful in photonic-based bio-medical applications as well as in material science. Thus, the fabrication of optically active surface-grafted spherical microspheres with these features should be highly promising for biomedical sciences. MCF-7 and A-549 cell lines with two different assays (MTT and NRU assays) were employed to determine the toxic potential of the as-designed PSMSs.

2. Experimental

2.1. Materials

Pr_3O_7 (BDH Chemicals, UK), was dissolved in dilute HNO_3 to convert it into $Pr(NO_3)_3{\cdot}6H_2O$. Tetraethyl-orthosilicate (TEOS), cetyltrimethylammonium bromide (CTAB), C_2H_5OH, and NaOH were analytical grade and used directly as received. Milli-Q (Millipore, Bedford, USA) H_2O was used for synthesis and characterization.

2.2. Synthesis of praseodymium encapsulated silica microspheres

In a typical synthesis, 0.3 g of NaOH and 1.0 g of CTAB were dissolved in 450 mL distilled water under constant stirring on a hot plate at 80 °C [3,9,41]. After homogeneous mixing, one mL of TEOS was injected slowly into the vigorously stirred hot solution for 2 h until a white precipitate was formed. Then 0.5 g of praseodymium nitrate hexahydrate dissolved in water was added dropwise into the mechanically stirred reaction mixture to form a surface coating of optically active $Pr(OH)_3$ shell over the silica spheres. The resulting white-greenish precipitate was separated by centrifugation, washed with distilled water and dried overnight in an oven at 60 °C, and then calcined in air at 500 °C for 3 h.

2.3. Characterization

The X-ray diffraction pattern was measured using a Rigaku-Dmax 2500 diffractometer equipped with *Cu Kα* ($\lambda = 1.54056$ Å) radiation for determination of chemical composition. Thermogravimetric analysis (TGA) was measured with a TGA/DTA Mettler Toledo AG, Analytical CH-8603, Schwerzenbach, Switzerland. Morphology was checked using a field emission scanning electron microscope (FE-SEM, JEOL, Japan) and field emission transmission electron microscope (FE-TEM, JEM-2100 F, JEOL, Japan); both were equipped for energy dispersive X-ray (EDX) analysis operating with an accelerating voltage of 200 kV. The Brunauer-Emmett-Teller (BET, Model: Barrett-Joyner-Halenda (BJH)) method was applied for measuring the specific surface area, porosity, and pore volume of the nanomaterials. Fourier transform infrared (FTIR) spectra were recorded by a Perkin-Elmer-580B IR spectrometer using the KBr pellet method. UV/vis absorption spectra were measured by a Cary 60 (Agilent Technologies, USA) UV/vis spectrophotometer in the spectral range 200–900 nm.

2.4. Cell viability via MTT and NRU assays

Cell viability was performed on two different cell lines using two different assays. Human breast cancer (MCF-7) and humane lung cancer cells (A-549) were employed for MTT and Neutral red uptake (NRU) assays. The MTT assay reveals the mitochondrial function, whereas an NRU assay represents the lysosome activity of living cells. A previous method was followed for the culture of both cell lines, which were stored in an incubator at 5% CO_2 and 37 °C for 24 h [3,42,47,48]. Briefly, 1×10^4 cells per well were grown in 96-well plates and treated with concentrations of 2, 5, 10, 25, 50, 100, and 200 μg/mL PSMSs for 24 h. After cell treatment, the culture medium was eliminated to avoid any interference of PSMSs and exchanged with a fresh medium comprising MTT solution in an amount equal to 10% and incubated for 24 h at 37 °C until the formation of purple formazan color. Finally, 96-well plates were centrifuged to settle out the remaining PSMSs. The variation in morphology of 96-well cell plates was investigated by an optical microscope for the different PSMSs concentrations.

2.5. Statistical analysis

Statistical analysis was performed followed by one-way Dunnett's multiple comparison method. The significance of the statistical study

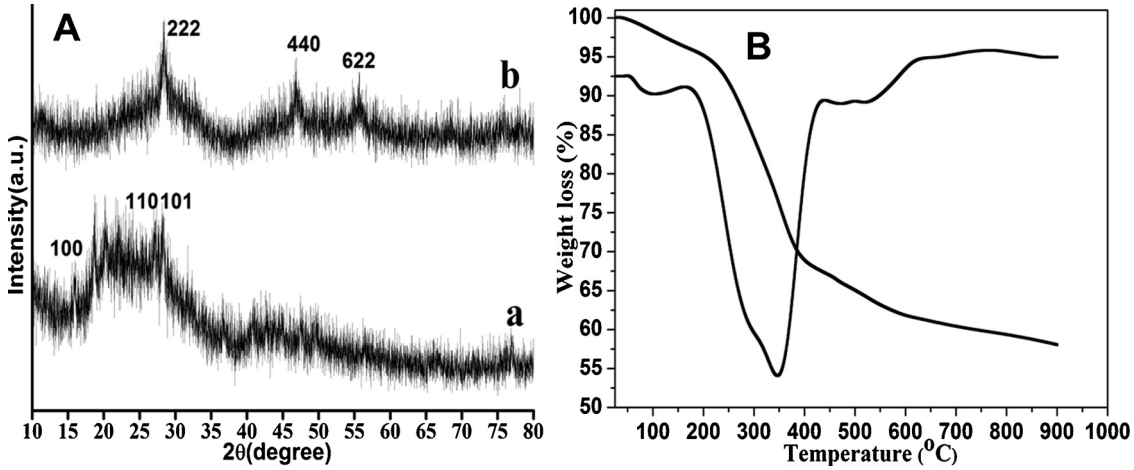

Fig. 1. (A) XRD pattern of PSMSs (a) after synthesis (b) after annealed at 500 °C and (B) TGA analysis of PSMSs.

was ascribed at $p \leq 0.05$.

3. Results and discussion

3.1. Crystallography and morphology

Phase formation and crystallinity of the as-prepared powder sample was determined from the X-ray diffraction pattern. The XRD pattern of the optically active powder in Fig. 1(A)a displays a broad band in the range 2θ = 20-35° along with well-resolved broad width reflection planes at 2θ = 16°, 27° and 28°, corresponding to the (100), (110), and (101) diffraction lines of hexagonal phase $Pr(OH)_3$, respectively [49–51]. An observed broad width reflection band at lower 2θ angles corresponds to the amorphous nature of silica microspheres (JCPDS card No. 29-0085) [39,52], in good agreement with previous reports [39,52–54]. As seen in Fig. 1(A)b, on annealing the sample at 500 °C the broadening of the silica reflection band is increased along with some new well-resolved diffraction planes, which can be indexed to the cubic phase of Pr_2O_3. This indicates that on annealing, the amorphous $Pr(OH)_3$ phase is converted into a crystalline phase of Pr_2O_3, which is successfully encapsulated on the surface of the silica spheres. However, the broadening of the diffraction planes suggests very low crystallinity of the material, which is consistent with previous reports [39,52,55]. We expected that a coating of optically active Pr^{3+} over a silica framework would expand the pore size and volume resulting in rearrangement of the Si − OH and Si-O-Si network structure, assisted by the electronic charge of the trivalent Pr ion [56]. As well, the broadening of the reflection peak width could be due to the surface coating of Pr^{3+} ion changing the structural Si–O bond distance and/or Si–O–Si angles [37]. Therefore, these results clearly suggest that the $Pr(OH)_3$ coating on the silica framework strongly interacts with the O atoms and changes the siliceous network structure [56]. As observed in Fig. 1(A)b, the diffraction plane width becomes broader after annealing, implying that the usual crystallite size of PSMSs becomes smaller than that of its respective un-annealed sample. It is known that PSMSs contain abundant surface-anchored hydroxyl groups and is either amorphous or ultra-small crystalline. Thus, on thermal treatment, conversion of $Pr(OH)_3$ into Pr_2O_3 would be blocked to some extent. Secondly, the formation of amorphous silica spheres suppresses the crystallinity, whereas crystal growth requires expansion of grain boundaries. These grain boundaries are trapped by the silica network, resulting in restricted motion by the introduction of tiny secondary-phase particles along grain boundaries. Here, we believe that silica microspheres serve as trapping particles for the rare-earth hydroxides.

Thermal stability and phase purity of the micro-powder was investigated by TGA analysis in the range 25–900 °C under a N_2 atmosphere. As seen in Fig. 1(B), the first mass loss (~6%) is observed between 25 and 170 °C with a DTA peak at 96 °C; this suggests dehydration of surface-adsorbed residual water molecules and organic moieties that are attached physically and chemically on the surface of the particles. A second step of decomposition is seen between 170 and 400 °C with a weight loss of 26%, and is attributed to the transformation of the amorphous form of the microspheres into crystalline SiO_2 [57,58]. It is further verified by the exothermic peak observed at 346 °C in the DTA curve. A third step of decomposition is observed between 400 and 600 °C with a mass loss of 7%. This could be due to combustion and elimination of carbon dioxide, as supported by the exothermic peak observed at 527 °C in the DTA curve. After this step, we observe slow weight loss of the precursor at higher temperatures; this indicates the complete conversion of the micro-powder into SiO_2 [45]. The TGA curve shows a residual mass of 57%, which accounts for the final silicon dioxide.

Morphological characterization was carried out using SEM and TEM micrographs. SEM images in Fig. 2A–C illustrate the mesoporous, mono-disperse, rough surface, the narrow size distribution, and uniform spherical hollow PSMSs but irregular size with an average grain size of about 500–700 nm. It is obvious from the low magnification image that the surface of each hollow PSMS consists of a large number of open pores of irregular shape and size, and this could be due to the removal of gaseous CO_2 when PSMSs are oxidized during the calcination process. Additionally, the high and low magnification SEM images in Fig. 2A–C demonstrate that each PSMS consists of small grains with a size of several nm. The morphological character was further examined from FE-TEM micrographs to verify the shape and size of the phosphor material. TEM images in Fig. 2D–E show monodisperse, irregularly sized, non-aggregated, spherical shapes with a narrow size distribution. The TEM images clearly display that the particles are closely interconnected, forming a random network, and the distribution of the pores is irregular. The average particle size was measured to be 650 nm and this is in good agreement with SEM results. Energy dispersive X-ray analysis (EDX) verified the presence of all the expected constituents in the as-designed hollow PSMSs. To further support the elemental composition of the hollow PSMSs, element mapping with a high-angle annular dark field and scanning transmission electron microscopy mode (HAADF-STEM) was performed, as shown in Fig. 3A–E. It clearly reveals the presence of silicon (Si), oxygen (O) and praseodymium (Pr) ions in the micro-products before and after calcination.

Specific surface area, porosity, pore size, and pore volume of the as-prepared nano-products were analyzed by nitrogen adsorption-desorption isotherm, shown in Fig. 4(A). It is an IV-like isotherm with an H_1-type hysteresis loop according to IUPAC classification, which is a well-known characteristic of mesoporous materials. The BET surface area,

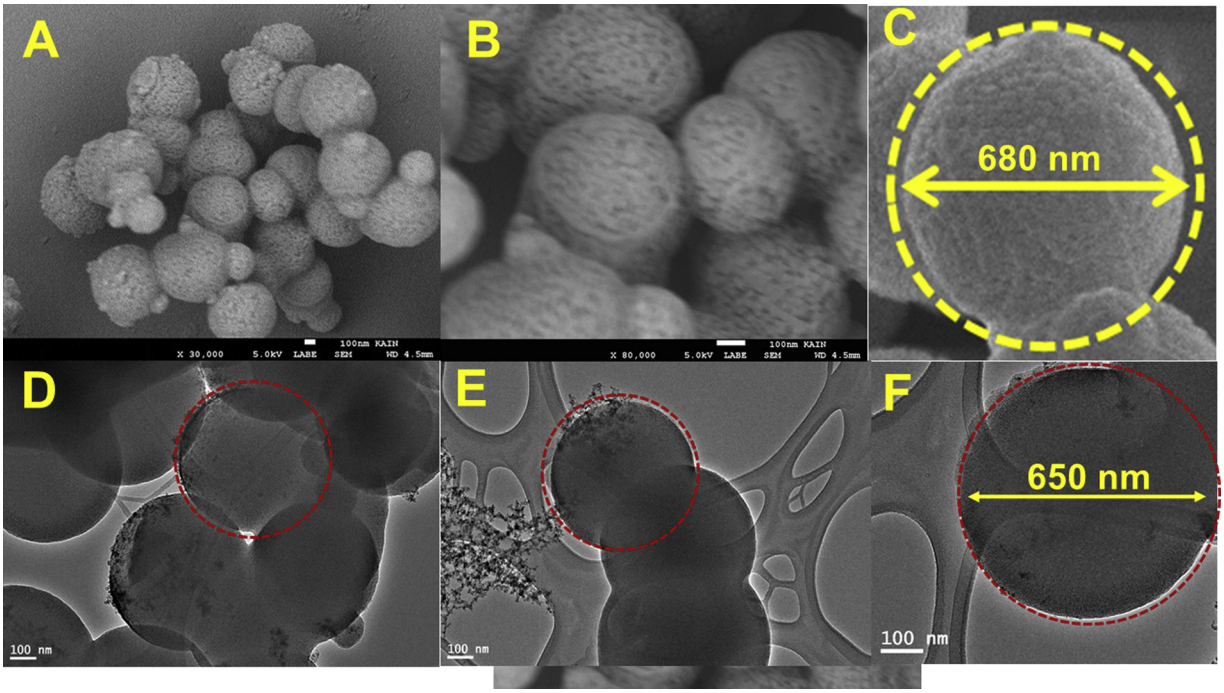

Fig. 2. SEM micrographs (A) low magnification (B) high magnification(C) single particle (D) TEM micrograph low magnification (E) high magnification and (F) single particle of PSMSs.

estimated BJH pore size, and pore volume were found to be 60.6 m^2/g, 198.02 Å, and 0.9962 cm^3/g, respectively. The large specific surface area and high porosity of the PSMSs cause expansion and passivation of the Si-O-Pr network along with charge balance over the surface of the silica PSMSs. This surface network distorts the crystallographic structure, changing bond angles and bond lengths due to the high electronegativity of the small Pr^{3+} ion, and increasing the imperfect packing of these particles. Some of the porosity may be related to cavities in hollow particles or interstitial spaces between nanoparticles in the shell. These observations are in good agreement with the results of XRD, TGA, SEM, TEM, and FTIR (Figs. 2 & 3). With the promising mesoporous characteristics of the as-designed optically active material, we have developed an effective approach that could be useful for the preparation of other porous fluorescent core-shell nanomaterials, and could be applied to prepare host material for storing drug molecules and fluorescent bio-probe/optical bio-sensors.

3.2. Optical properties

The surface chemistry of the as-prepared nano-products was determined by FTIR analysis. Fig. 4(B) shows the infrared spectrum of the nanospheres. The occurrence of a diffuse intensity infrared band at around 3443 cm^{-1} along with a weak intensity band located at 1643 cm^{-1} corresponds to the stretching and bending vibrational modes of hydroxyl groups covering the surface, indicating that the surface is covered with a $Pr(OH)_3$ layer. The strong doublet peak at around 1090 cm^{-1} with two weak intensity peaks located at 971 and 794 cm^{-1} originate from Si-O-Si, Si-O, and Si − OH stretching & bending vibrational modes, respectively, of amorphous silica [2,4,41,59]. The weak intensity sharp band observed at 470 cm^{-1} suggests the construction of a metal-oxygen (Si-O-Pr) network over the surface of the core spheres [41,43,45]. These observations agree well with XRD, TGA and EDX analysis.

UV/vis spectroscopy was carried out to examine the optical properties, aqueous dispersibility, and colloidal stability at ambient conditions. Fig. 5 displays the absorption spectrum of Pr^{3+} functionalized silica PSMSs along with pure phase silica spheres [4,41] and Pr $(NO_3)_3.6H_2O$ in water within the UV/vis range 200–700 nm for comparison purposes. As seen in Fig. 5, the optical absorption spectrum of PSMSs reveals well-known $^3P_2$, $^3P_1$, $^3P_0$ and $^1D_2$ weak intensity absorption transitions of the Pr(III) ion [60], confirming the presence of the Pr^{3+} ion on the surface of the PSMSs. The intensity of the Pr^{3+} ion absorption transitions is very weak because of the high absorbance by optically active silica PSMSs [4,41].

3.3. Cytotoxicity by MTT assay

An MTT assay was employed to examine the mitochondrial function and membrane leakage to evaluate cell viability upon treatment of serum cells with PSMSs. Two different types of cell line, MCF-7 and A-549, were incubated with PSMSs at concentrations of 2, 5, 10, 25, 50, 100, and 200 µg/mL for 24 h (Fig. 6A&B). The PSMSs along with both cell lines in the control experiment do not reveal any appreciable reduction in cell proliferation up to 24 h. As shown in Fig. 6 > 90% of the cells are viable up to a concentration of 25 µg/mL. At higher concentrations of PSMSs the cell viability is suppressed, but up to 100 µg/mL of PSMSs there is still > 70% viability, even after incubation for 24 h. At 200 µg/mL of PSMSs, the cell viability in both serum cells is further quenched but retains 55–60% viability. We expect that on increasing the dose of the PSMSs, some non-coordinated surface hydroxyl groups enhance the concentration of free hydroxyl groups, which may be responsible for the reduction in cell viability resulting in enhanced toxicity.

3.4. Cytotoxicity by NRU assay

Toxicity was further examined by NRU assay to validate the toxic potential of the as-prepared PSMSs (Fig. 7A & B). Both MCF-7 and A-549 cell lines were exposed to various concentrations of as-prepared PSMSs to determine cell vitality. The cell viability for both cell lines is more than 75% up to 50 µg/mL concentration of PSMSs even after incubation for 24 h. Similar to what was observed in the MTT assay, the cell viability in the NRU assay is significantly reduced on increasing the dose of PSMSs. This could be due to an increase of released free radicals

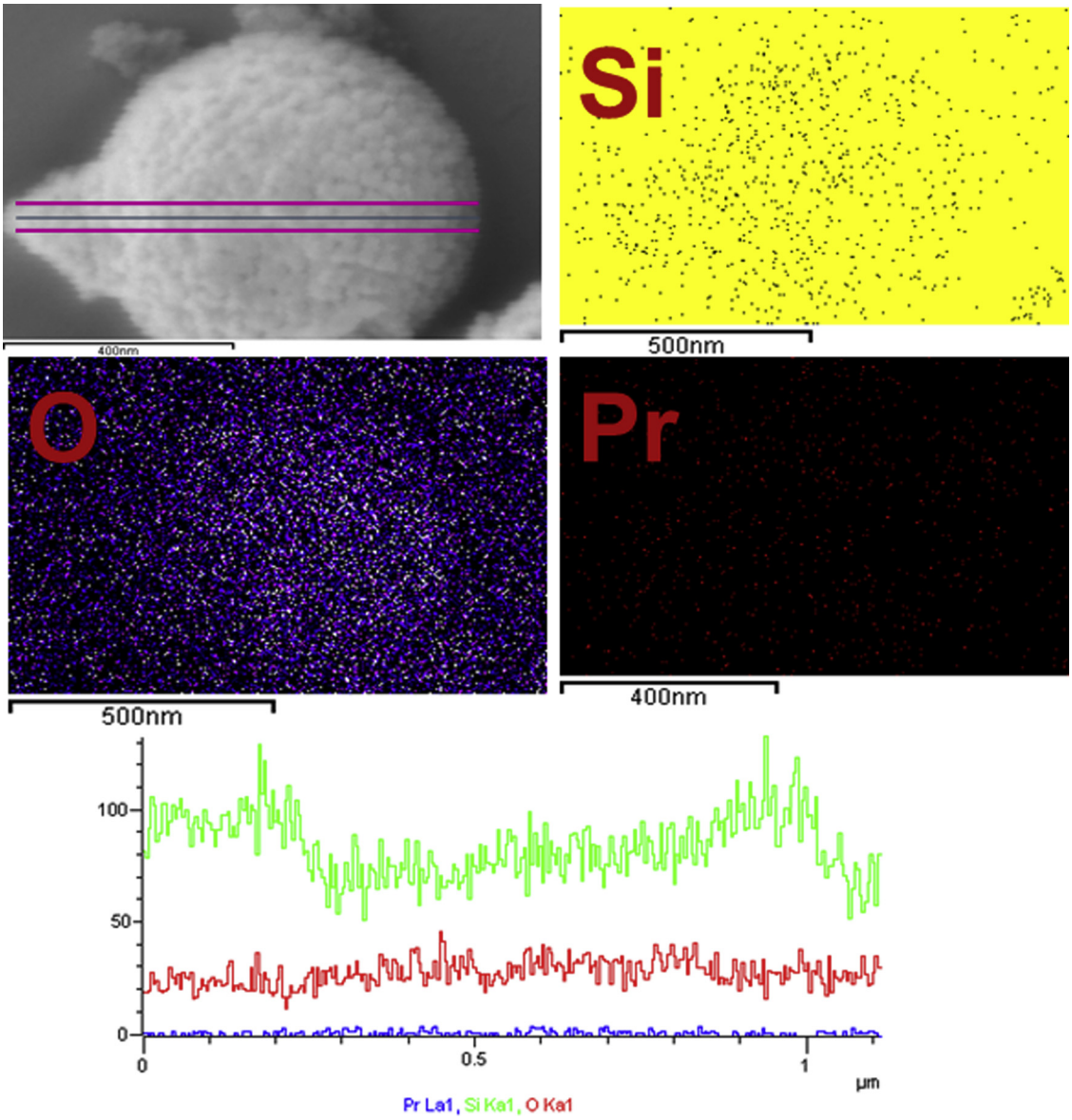

Fig. 3. Line mapping from high-angle annular dark field &FE-SEM mode of each elements in PSMSs.

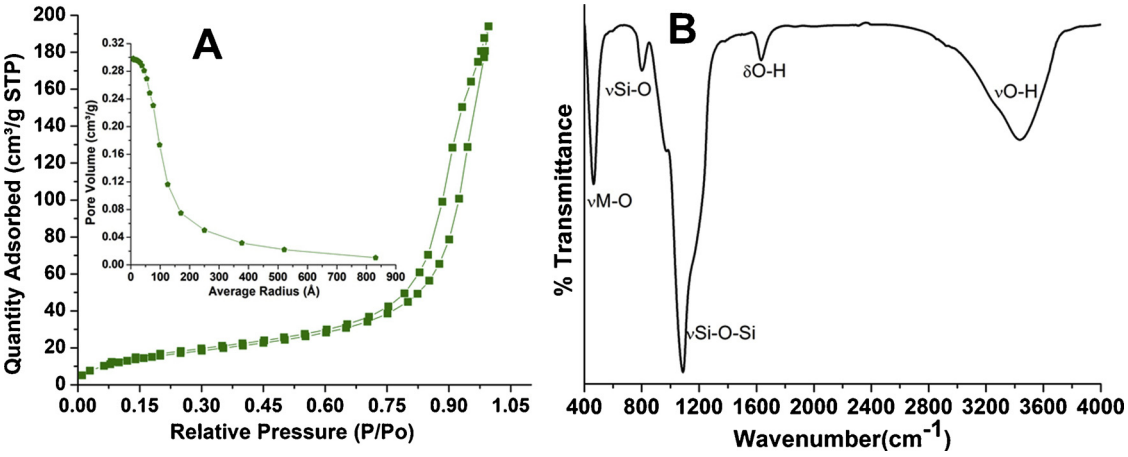

Fig. 4. (A) N_2-adsorption-desorption and inset pore size distribution curve of PSMSs and (B) FTIR spectrum of PSMSs.

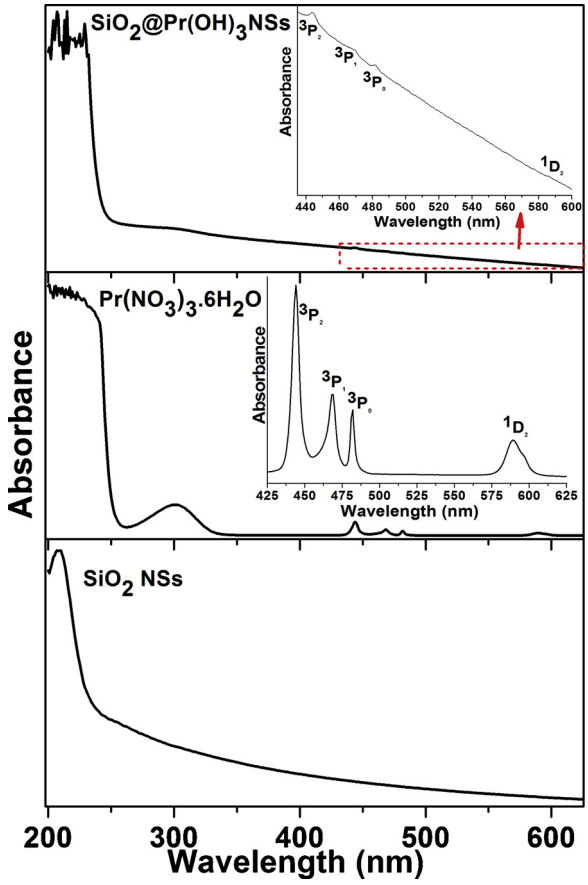

Fig. 5. UV/vis spectra of SiO_2, $Pr(NO_3)_36H_2O$(inset high resolution) and PSMSs (inset high resolution) PSMSs.

from the PSMSs which suppress cell proliferation; these observations are in accord with the MTT assay results.

3.5. Morphological evaluation

Optical microscopy was applied to investigate the interaction of living cells with as-designed PSMSs (Fig. 8(A & B). Optical microscopic images were obtained for both cell lines as a function of dosage after incubation for 24 h. Both cell lines were incubated for 24 h with various concentrations of PSMSs to determine the impact of various PSMSs concentrations on cell morphology. As seen in Fig. 8(A&B), cells are spread out in the control experiment as well as at low concentrations of PSMSs and begin to proliferate. On increasing the dosage of PSMSs from 10 to 100 μg/mL, the cell lines are slightly scattered. A further increase in concentration from 100 to 200 μg/mL results in the cell lines being highly scattered and their density is gradually reduced. The reduction in cell viability and splitting of cell colonies (optical images) at the high dosage of PSMSs indicates that some non-covalently bonded or excess hydroxyl groups are produced in aqueous solution, affecting the pH value of the medium. These excess amounts produce hydroxyl groups in the form of free radicals which kill cells and suppress the cell viability. Additionally, lanthanides are small in size and represent a high coordination number. Because of the high coordination number, some non-bonded hydroxyl groups or OH– groups attracted by van der Waals forces in aqueous solution are easily released and increase the OH– concentration, resulting in a change in the pH of the solution. The high concentration of OH radicals in aqueous solution increases the basicity, causing the cells either to precipitate or aggregate. The optical microscopy images in Fig. 8(A & B) at a high dose of PSMSs clearly support the above conclusions.

4. Conclusions

In summary, $Pr(OH)_3$-grafted silica microspheres were successfully prepared by a heat-treated sol-gel chemical process at low temperature. XRD results illustrate semi-amorphous or ultra-small crystalline PSMSs. The morphology of the obtained MSs is mesoporous, monodisperse, well-connected, rough-surfaced, and spherical, but with irregular size and narrow size distribution. N_2-adsorption-desorption isotherm analysis show that there is a large specific surface area with broad pore size distribution. Optical absorption spectra reveal high aqueous dispersibility and good colloidal stability in aqueous media along with weak absorption transitions of Pr^{3+} ion in the visible region because of the influence of silica. The MTT assay, NRU assay, and morphological results revealed high cell viability, i.e. nontoxicity up to a certain concentration range on both cell lines in both assays. At a high concentration range, hydroxyl radicals were produced resulting in suppression of cell viability. The high aqueous colloidal stability, chemical inertness, good biocompatibility, and non-toxic behavior of these PSMSs make them a promising candidate for their future use in biomedical and drug delivery applications.

Acknowledgment

The authors extend their sincere appreciation to the Deanship of

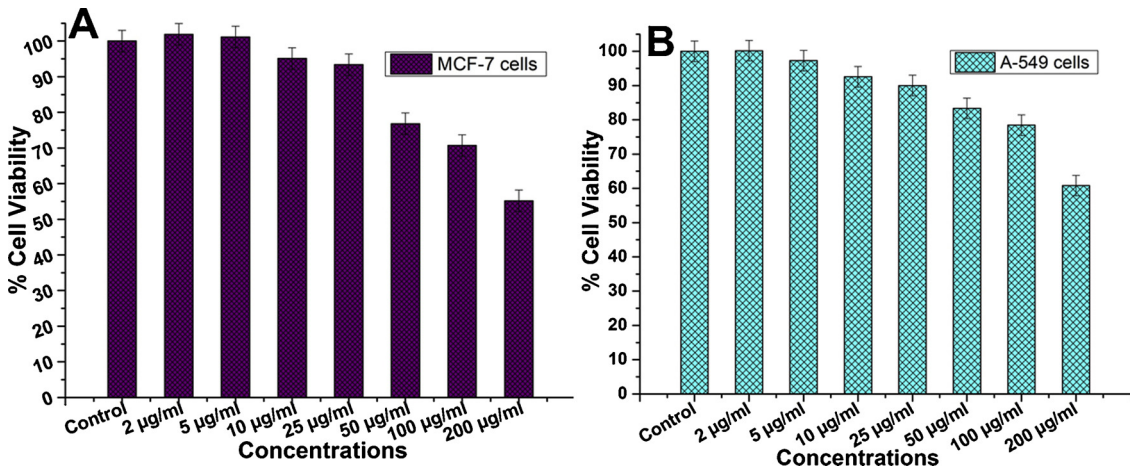

Fig. 6. Cytotoxicity assessment by MTT assay on (**A**) MCF-7and (**B**) A-549 cell lines for PSMSs. Cells were exposed optically active PSMSs at 2–200 mg/mL for 24 h. Results are presented as mean + SD from three independent experiments.

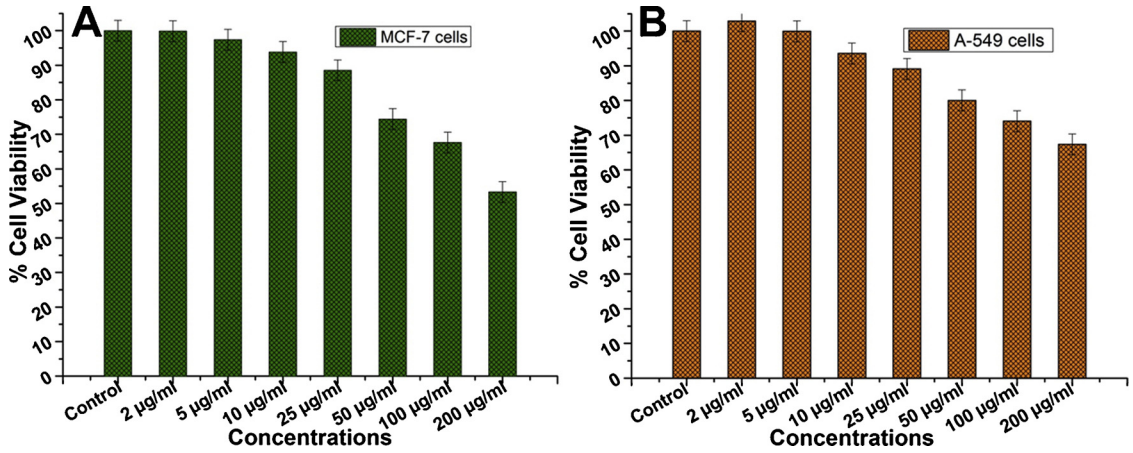

Fig. 7. Cytotoxicity assessment by neutral red uptake (NRU) assay on (**A**) MCF-7and (**B**) A-549 cell lines for PSMSs. Cells were exposed optically active PSMSs at 2–200 mg/mL for 24 h. Results are presented as mean + SD from three independent experiments.

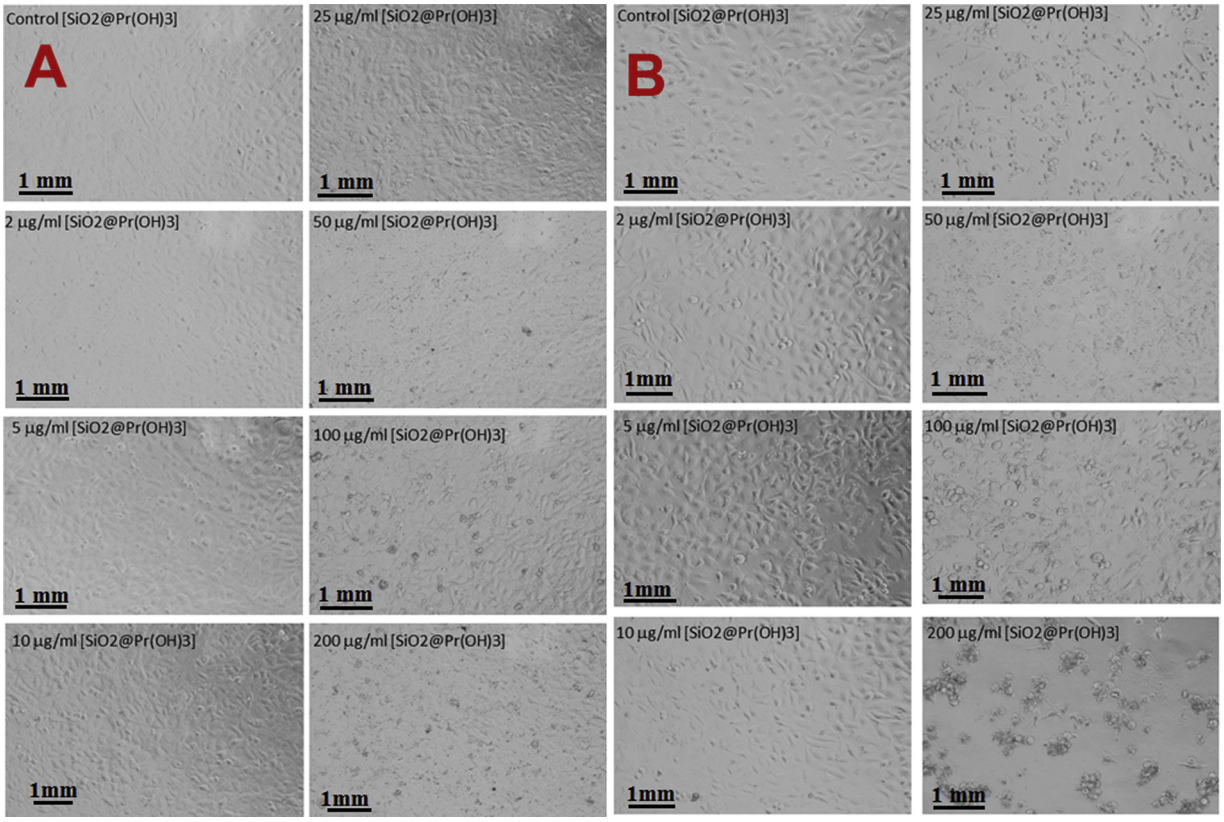

Fig. 8. Morphological alterations in [A] MCF-7 and [B] A-549 cells exposed to PSMSs at 2–200 mg/mL for 24 h. Micrographs were taken using phase contrast inverted microscope at 20× magnification.

Scientific Research at King Saud University, Riyadh for funding this work through Research Group No. (RG-1439-089).

References

[1] F.Q. Tang, L.L. Li, D. Chen, Mesoporous silica nanoparticles: synthesis, biocompatibility and drug delivery, Adv. Mater. 24 (2012) 1504–1534.
[2] A.A. Ansari, M. Alam, J.P. Labis, S.A. Alrokayan, G. Shafi, T.N. Hasan, N.A. Syed, A.A. Alshatwi, Luminescent mesoporous LaVO4:Eu3+ core-shell nanoparticles: synthesis, characterization, biocompatibility and their cytotoxicity, J. Mater. Chem. 21 (2011) 19310–19316.
[3] A.A. Ansari, A. Aldalbahi, J.P. Labis, A.M. El-Toni, M. Ahamed, M.A. Manthrammel, Colloid Surf. B 163 (2018) 133–139.
[4] A.A. Ansari, J.P. Labis, One-pot synthesis and photoluminescence properties of luminescent functionalized mesoporous SiO2@Tb(OH)(3) core-shell nanospheres, J. Mater. Chem. 22 (2012) 16649–16656.
[5] S.L. Gai, P.P. Yang, C.X. Li, W.X. Wang, Y.L. Dai, N. Niu, J. Lin, Synthesis of magnetic, up-conversion luminescent, and mesoporous core-shell-structured nanocomposites as drug carriers, Adv. Funct. Mater. 20 (2010) 1166–1172.
[6] S.L. Gai, P.P. Yang, D. Wang, C.X. Li, N. Niu, F. He, M.L. Zhang, J. Lin, Luminescence functionalization of MCM-48 by YVO4:Eu3+ for controlled drug delivery, RSC Adv. 2 (2012) 3281–3287.
[7] M.K. Gnanasammandhan, N.M. Idris, A. Bansal, K. Huang, Y. Zhang, Near-IR photoactivation using mesoporous silica-coated NaYF4:Yb,Er/Tm upconversion nanoparticles, Nat. Protoc. 11 (2016) 688–713.
[8] S.S. Huang, Y. Fan, Z.Y. Cheng, D.Y. Kong, P.P. Yang, Z.W. Quan, C.M. Zhang, J. Lin, Magnetic mesoporous silica spheres for drug targeting and controlled release, J. Phys. Chem. C 113 (2009) 1775–1784.
[9] I.I. Slowing, B.G. Trewyn, V.S.Y. Lin, Mesoporous silica nanoparticles for intracellular delivery of membrane-impermeable proteins, J. Am. Chem. Soc. 129 (2007) 8845–8849.
[10] Y.L. Dai, H.T. Bi, X.R. Deng, C.X. Li, F. He, P.A. Ma, P.P. Yang, J. Lin, 808 nm near-infrared light controlled dual-drug release and cancer therapy in vivo by

upconversion mesoporous silica nanostructures, J. Mater. Chem. B 5 (2017) 2086–2095.
[11] D.A. Eurov, D.A. Kurdyukov, D.A. Kirilenko, J.A. Kukushkina, A.V. Nashchekin, A.N. Smirnov, V.G. Golubev, Core-shell monodisperse spherical mSiO(2)/Gd2O3:Eu3+@mSiO(2) particles as potential multifunctional theranostic agents, J. Nanopart. Res. 17 (2015).
[12] L.L. Feng, F. He, Y.L. Dai, S.L. Gai, C.N. Zhong, C.X. Li, P.P. Yang, Multifunctional UCNPs@MnSiO3@g-C3N4 nano-platform: improved ROS generation and reduced glutathione levels for highly efficient photodynamic therapy, Biomater. Sci. 5 (2017) 2456–2467.
[13] S.L. Gai, P.P. Yang, J.G. Hao, W.X. Wang, N. Niu, F. He, D. Wang, J. Lin, Fabrication of luminescent and mesoporous core-shell structured nanocomposites and their application as drug carrier, Microporous Mesoporous Mater. 131 (2010) 128–135.
[14] S.L. Gai, P.P. Yang, P.A. Ma, D. Wang, C.X. Li, X.B. Li, N. Niu, J. Lin, Fibrous-structured magnetic and mesoporous Fe3O4/silica microspheres: synthesis and intracellular doxorubicin delivery, J. Mater. Chem. 21 (2011) 16420–16426.
[15] X.M. Li, L. Zhou, Y. Wei, A.M. El-Toni, F. Zhang, D.Y. Zhao, Anisotropic growth-induced synthesis of dual-compartment Janus mesoporous silica nanoparticles for bimodal triggered drugs delivery, J. Am. Chem. Soc. 136 (2014) 15086–15092.
[16] X.H. Liang, J. Fan, Y.B. Wang, Y.Y. Zhao, R.Y. Jin, T. Sun, M. Cheng, X.J. Wang, Synthesis of hollow and mesoporous structured NaYF4:Yb,Er upconversion luminescent nanoparticles for targeted drug delivery, J. Rare Earth 35 (2017) 419–429.
[17] B. Liu, C.X. Li, D.M. Yang, Z.Y. Hou, P.A. Ma, Z.Y. Cheng, H.Z. Lian, S.S. Huang, J. Lin, Upconversion-luminescent core/mesoporous-silica-shell structured beta-NaYF4:Yb3+,Er3+@SiO2@mSiO(2) composite nanospheres: fabrication and drug-storage/release properties, Eur. J. Inorg. Chem. 2014 (2014) 1906–1913.
[18] R.C. Lv, P.P. Yang, F. He, S.L. Gai, C.X. Li, Y.L. Dai, G.X. Yang, J. Lin, A yolk-like multifunctional platform for multimodal imaging and synergistic therapy triggered by a single near-infrared light, ACS Nano 9 (2015) 1630–1647.
[19] N. Niu, F. He, P.A. Ma, S.L. Gai, G.X. Yang, F.Y. Qu, Y. Wang, J. Xu, P.P. Yang, Up-conversion nanoparticle assembled mesoporous silica composites: synthesis, plasmon-enhanced luminescence, and near-infrared light triggered drug release, ACS Appl. Mater. Interfaces 6 (2014) 3250–3262.
[20] D.K. Shen, J.P. Yang, X.M. Li, L. Zhou, R.Y. Zhang, W. Li, L. Chen, R. Wang, F. Zhang, D.Y. Zhao, Biphase stratification approach to three-dimensional dendritic biodegradable mesoporous silica nanospheres, Nano Lett. 14 (2014) 923–932.
[21] J.T. Xu, F. He, Z.Y. Cheng, R.C. Lv, Y.L. Dai, A. Gulzar, B. Liu, H.T. Bi, D. Yang, S.L. Gai, P.P. Yang, J. Lin, Yolk-structured upconversion nanoparticles with biodegradable silica shell for FRET sensing of drug release and imaging-guided chemotherapy, Chem. Mater. 29 (2017) 7615–7628.
[22] J.T. Xu, D. Yang, R.C. Lv, B. Liu, S.L. Gai, F. He, C.X. Li, P.P. Yang, Design, fabrication, luminescence and biomedical applications of UCNPs@mSiO(2)-ZnPc-CDs-P(NIPAm-MAA) nanocomposites, J. Mater. Chem. B 4 (2016) 5883–5894.
[23] J.T. Xu, P.P. Yang, M.D. Sun, H.T. Bi, B. Liu, D. Yang, S.L. Gai, F. He, J. Lin, Highly emissive dye-sensitized upconversion nanostructure for dual-photosensitizer photodynamic therapy and bioimaging, ACS Nano 11 (2017) 4133–4144.
[24] Z.H. Xu, Y. Gao, S.S. Huang, P.A. Ma, J. Lin, J.Y. Fang, A luminescent and mesoporous core-shell structured Gd2O3:Eu3+@nSiO(2)@mSiO(2) nanocomposite as a drug carrier, Dalton Trans. 40 (2011) 4846–4854.
[25] G.X. Yang, D. Yang, P.P. Yang, R.C. Lv, C.X. Li, C.N. Zhong, F. He, S.L. Gai, J. Lin, A single 808 nm near-infrared light-mediated multiple imaging and photodynamic therapy based on titania coupled upconversion nanoparticles, Chem. Mater. 27 (2015) 7957–7968.
[26] J.P. Yang, D.K. Shen, L. Zhou, W. Li, X.M. Li, C. Yao, R. Wang, A.M. El-Toni, F. Zhang, D.Y. Zhao, Spatially confined fabrication of core-shell gold nanocages@mesoporous silica for near-infrared controlled photothermal drug release, Chem. Mater. 25 (2013) 3030–3037.
[27] P.P. Yang, Z.W. Quan, Z.Y. Hou, C.X. Li, X.J. Kang, Z.Y. Cheng, J. Lin, A magnetic, luminescent and mesoporous core-shell structured composite material as drug carrier, Biomaterials 30 (2009) 4786–4795.
[28] L. Zhou, Z.W. Chen, K. Dong, M.L. Yin, J.S. Ren, X.G. Qu, DNA-mediated construction of hollow upconversion nanoparticles for protein harvesting and near-infrared light triggered release, Adv. Mater 26 (2014) 2424–2430.
[29] X.J. Kang, Z.Y. Cheng, C.X. Li, D.M. Yang, M.M. Shang, P.A. Ma, G.G. Li, N.A. Liu, J. Lin, Core-shell structured up-conversion luminescent and mesoporous NaYF4:Yb3+/Er3+@nSiO(2)@mSiO(2) nanospheres as carriers for drug delivery, J. Phys. Chem. C 115 (2011) 15801–15811.
[30] C.X. Li, Z.Y. Hou, Y.L. Dai, D.M. Yang, Z.Y. Cheng, P.A. Ma, J. Lin, A facile fabrication of upconversion luminescent and mesoporous core- shell structured beta-NaYF4:Yb3+, Er3+@mSiO(2) nanocomposite spheres for anti-cancer drug delivery and cell imaging, Biomater. Sci. 1 (2013) 213–223.
[31] C.K. Lin, H. Wang, D.Y. Kong, M. Yu, X.M. Liu, Z.L. Wang, J. Lin, Silica supported submicron SiO2@Y2SiO5: Eu3+ and SiO2@Y2SiO5 : Ce3+/Tb3+ spherical particles with a core-shell structure: sol-gel synthesis and characterization, Eur. J. Inorg. Chem. (2006) 3667–3675.
[32] Y. Wu, D.M. Yang, X.J. Kang, P.A. Ma, S.S. Huang, Y. Zhang, C.X. Li, J. Lin, Core-shell structured luminescent and mesoporous beta-NaYF4:Ce3+/Tb3+@mSiO(2)-PEG nanospheres for anti-cancer drug delivery, Dalton Trans. 42 (2013) 9852–9861.
[33] P.P. Yang, Z.W. Quan, L.L. Lu, S.S. Huang, J. Lin, Luminescence functionalization of mesoporous silica with different morphologies and applications as drug delivery systems, Biomaterials 29 (2008) 692–702.
[34] H. Matsushita, S. Mizukami, F. Sugihara, Y. Nakanishi, Y. Yoshioka, K. Kikuchi, Angew. Chem. Int. Ed. 53 (2014) 1008–1011.
[35] G.X. Yang, R.C. Lv, S.L. Gai, Y.L. Dai, F. He, P.P. Yang, Multifunctional SiO2@Gd2O3:Yb/Tm hollow capsules: controllable synthesis and drug release properties, Inorg. Chem. 53 (2014) 10917–10927.
[36] Y. Chen, H.R. Chen, Y. Sun, Y.Y. Zheng, D.P. Zeng, F.Q. Li, S.J. Zhang, X. Wang, K. Zhang, M. Ma, Q.J. He, L.L. Zhang, J.L. Shi, Multifunctional mesoporous composite nanocapsules for highly efficient MRI-Guided high-intensity focused ultrasound cancer surgery, Angew. Chem. Int. Ed. 50 (2011) 12505–12509.
[37] J. Kim, H.S. Kim, N. Lee, T. Kim, H. Kim, T. Yu, I.C. Song, W.K. Moon, T. Hyeon, Multifunctional uniform nanoparticles composed of a magnetite nanocrystal core and a mesoporous silica shell for magnetic resonance and fluorescence imaging and for drug delivery, Angew. Chem. Int. Ed. 47 (2008) 8438–8441.
[38] Y.S. Lin, Y. Hung, H.Y. Lin, Y.H. Tseng, Y.F. Chen, C.Y. Mou, Photonic crystals from monodisperse lanthanide-hydroxide-at-silica core/shell colloidal spheres, Adv. Mater. 19 (2007) 577.
[39] M. Yu, J. Lin, J. Fang, Silica spheres coated with YVO4 : Eu3+ layers via sol-gel process: a simple method to obtain spherical core-shell phosphors, Chem. Mater. 17 (2005) 1783–1791.
[40] R.C. Lv, P.P. Yang, B. Hu, J.T. Xu, W.T. Shang, J. Tian, In situ growth strategy to integrate up-conversion nanoparticles with ultrasmall CuS for photothermal theranostics, ACS Nano 11 (2017) 1064–1072.
[41] A.A. Ansari, T.N. Hasan, N.A. Syed, J.P. Labis, A.K. Parchur, G. Shafi, A.A. Alshatwi, In-vitro cyto-toxicity, geno-toxicity, and bio-imaging evaluation of one-pot synthesized luminescent functionalized mesoporous SiO2@Eu(OH)(3) core-shell microspheres, Nanomed. Nanotechnol. 9 (2013) 1328–1335.
[42] A.A. Ansari, A. Khan, J.P. Labis, M. Alam, M. Aslam Manthrammel, M. Ahamed, M.J. Akhtar, A. Aldalbahi, H. Ghaithan, Mesoporous multi-silica layer-coated Y2O3:Eu core-shell nanoparticles: synthesis, luminescent properties and cytotoxicity evaluation, Mater. Sci. Eng.: C 96 (2019) 365–373.
[43] A.A. Ansari, J.P. Labis, M.A. Manthrammel, Designing of luminescent GdPO4:Eu@LaPO4@SiO2 core/shell nanorods: synthesis, structural and luminescence properties, Solid State Sci. 71 (2017) 117–122.
[44] A.A. Ansari, J.P. Labis, M.A. Manthrammel, Synthesis, structural, and photoluminescence studies of LaF3:Pr, LaF3:Pr@LaF3, and LaF3:Pr@LaF3@SiO2 nanophosphors, J. Aust. Ceram. Soc. 54 (2018) 493–500.
[45] A.A. Ansari, A.K. Parchur, M. Alam, J. Labis, A. Azzeer, Influence of surface coating on structural and photoluminescent properties of CaMoO4:Pr nanoparticles, J. Fluoresc. 24 (2014) 1253–1262.
[46] A.A. Ansari, A.K. Aldalbahi, J.P. Labis, M.A. Manthrammel, Impact of surface coating on physical properties of europium-doped gadolinium fluoride microspheres, J. Fluorine Chem. 199 (2017) 7–13.
[47] T. Mosmann, Rapid colorimetric assay for cellular growth and survival - application to proliferation and cyto-toxicity assays, J. Immunol. Methods 65 (1983) 55–63.
[48] M. Ahamed, M.J. Akhtar, M.A. Siddiqui, J. Ahmad, J. Musarrat, A.A. Al-Khedhairy, M.S. AlSalhi, S.A. Alrokayan, Oxidative stress mediated apoptosis induced by nickel ferrite nanoparticles in cultured A549 cells, Toxicology 283 (2011) 101–108.
[49] J.G. Kang, B.K. Min, Y. Sohn, Physicochemical properties of praseodymium hydroxide and oxide nanorods, J. Alloys. Compd. 619 (2015) 165–171.
[50] R. Si, Y.W. Zhang, L.P. You, C.H. Yan, Rare-earth oxide nanopolyhedra, nanoplates, and nanodisks, Angew. Chem. Int. Ed. 44 (2005) 3256–3260.
[51] X. Wang, Y.D. Li, Synthesis and characterization of lanthanide hydroxide single-crystal nanowires, Angew. Chem. Int. Ed. 41 (2002) 4790–4793.
[52] H. Wang, C.K. Lin, X.M. Liu, J. Lin, M. Yu, Monodisperse spherical core-shell-structured phosphors obtained by functionalization of silica spheres with Y2O3 : Eu3+ layers for field emission displays, Appl. Phys. Lett. 87 (2005).
[53] M.Q. Tan, Z.Q. Ye, G.L. Wang, J.L. Yuan, Preparation and time-resolved fluorometric application of luminescent europium nanoparticles, Chem. Mater. 16 (2004) 2494–2498.
[54] Z.Q. Ye, M.Q. Tan, G.L. Wang, J.L. Yuan, Novel fluorescent europium chelate-doped silica nanoparticles: preparation, characterization and time-resolved fluorometric application, J. Mater. Chem. 14 (2004) 851–856.
[55] S. Santra, R. Tapec, N. Theodoropoulou, J. Dobson, A. Hebard, W.H. Tan, Synthesis and characterization of silica-coated iron oxide nanoparticles in microemulsion: the effect of nonionic surfactants, Langmuir 17 (2001) 2900–2906.
[56] T.S. Atabaev, H.K. Kim, Y.H. Hwang, Submicron Y2O3 particles codoped with Eu and Tb ions: size controlled synthesis and tuning the luminescence emission, J. Colloid Interface Sci. 373 (2012) 14–19.
[57] Z.H. Xu, Y. Guo, T. Liu, L.M. Wang, S.S. Bian, J. Lin, General and facile method to fabricate uniform Y2O3:Ln(3+) (Ln(3+) = Eu-3+,Eu- Tb3+) hollow microspheres using polystyrene spheres as templates, J. Mater. Chem. 22 (2012) 21695–21703.
[58] G.A. Jia, H.P. You, Y.H. Song, Y.J. Huang, M. Yang, H.J. Zhang, Facile synthesis and luminescence of uniform Y2O3 hollow spheres by a sacrificial template route, Inorg. Chem. 49 (2010) 7721–7725.
[59] T. Liu, W. Xu, X. Bai, H.W. Song, Tunable silica shell and its modification on photoluminescent properties of Y2O3:Eu3+@SiO2 nanocomposites, J. Appl. Phys. 111 (2012).
[60] A.A. Ansari, N. Singh, A.F. Khan, S.P. Singh, K. Iftikhar, Solvent effect on optical properties of hydrated lanthanide tris-acetylacetone, J. Lumin. 127 (2007) 446–452.